nature medicine

CYP3A5 mediates basal and acquired therapy resistance in different subtypes of pancreatic ductal adenocarcinoma

Elisa M Noll[1,2,16], Christian Eisen[1,2,16], Albrecht Stenzinger[3,4,15], Elisa Espinet[1,2], Alexander Muckenhuber[3,15], Corinna Klein[1], Vanessa Vogel[1], Bernd Klaus[5], Wiebke Nadler[1,2], Christoph Rösli[1,15], Christian Lutz[6], Michael Kulke[6], Jan Engelhardt[1,2], Franziska M Zickgraf[1,2], Octavio Espinosa[7], Matthias Schlesner[7], Xiaoqi Jiang[8], Annette Kopp-Schneider[8], Peter Neuhaus[9], Marcus Bahra[9], Bruno V Sinn[10], Roland Eils[7,11,12], Nathalia A Giese[13], Thilo Hackert[13], Oliver Strobel[13], Jens Werner[13,15], Markus W Büchler[13,14], Wilko Weichert[3,4,14,15], Andreas Trumpp[1,2,14,17] & Martin R Sprick[1,2,14,17]

Although subtypes of pancreatic ductal adenocarcinoma (PDAC) have been described, this malignancy is clinically still treated as a single disease. Here we present patient-derived models representing the full spectrum of previously identified quasi-mesenchymal (QM-PDA), classical and exocrine-like PDAC subtypes, and identify two markers—HNF1A and KRT81—that enable stratification of tumors into different subtypes by using immunohistochemistry. Individuals with tumors of these subtypes showed substantial differences in overall survival, and their tumors differed in drug sensitivity, with the exocrine-like subtype being resistant to tyrosine kinase inhibitors and paclitaxel. Cytochrome P450 3A5 (CYP3A5) metabolizes these compounds in tumors of the exocrine-like subtype, and pharmacological or short hairpin RNA (shRNA)-mediated CYP3A5 inhibition sensitizes tumor cells to these drugs. Whereas hepatocyte nuclear factor 4, alpha (*HNF4A*) controls basal expression of *CYP3A5*, drug-induced *CYP3A5* upregulation is mediated by the nuclear receptor *NR1I2*. CYP3A5 also contributes to acquired drug resistance in QM-PDA and classical PDAC, and it is highly expressed in several additional malignancies. These findings designate CYP3A5 as a predictor of therapy response and as a tumor cell–autonomous detoxification mechanism that must be overcome to prevent drug resistance.

PDAC is a very aggressive disease with poor prognosis[1]. In both Europe and the USA, pancreatic cancer is the fourth leading cause of cancer deaths[2,3]. Treatment with gemcitabine[4], the FOLFIRINOX scheme (a combination of oxaliplatin, irinotecan, fluorouracil and leucovorin)[5] or the nanoparticle albumin-bound paclitaxel (nab-paclitaxel)[6] offer only a modest increase in overall survival. Despite extensive testing of targeted therapies in clinical trials, all of the examined compounds confer little or no survival benefit in unselected cohorts of individuals with PDAC[1,7,8].

Although patient stratification according to molecular characteristics has not yet been performed in clinical trials for PDAC, transcriptional profiling of whole-tumor tissues suggest the existence of subtypes of PDAC that differ in patient survival and tumor metastasis[9,10]. Additionally, three PDAC subtypes (classical, QM-PDA and exocrine-like)[11] were described on the basis of gene expression profiling analyses of laser capture–microdissected epithelial tumors. However, in a larger panel of human and mouse PDAC cell lines, only the classical and the QM-PDA subtypes were identified[11], suggesting that currently used PDAC cell lines inadequately represent the heterogeneity of human PDAC. In addition, the classical and QM-PDA subtypes were suggested to differ in their responses to a range of chemotherapeutics, and the drug sensitivity of the exocrine-like subtype has yet to be determined[11].

Although resistance of PDAC to therapy is well described[1], little is known about the molecular mechanisms mediating it. Members of the cytochrome P450 (CYP) enzyme family have been previously investigated only with regards to a role in systemic drug metabolism[12,13] or their up- or downregulation in solid tumors as compared to normal tissues[14]. Thus, the functional role and impact of CYPs on tumor cell–autonomous drug resistance remains mostly unknown[14,15].

[1]Heidelberg Institute for Stem Cell Technology and Experimental Medicine (HI-STEM), Heidelberg, Germany. [2]Divison of Stem Cells and Cancer, German Cancer Research Center (DKFZ), Heidelberg, Germany. [3]Department of Pathology, University of Heidelberg, Heidelberg, Germany. [4]National Center for Tumor Diseases (NCT), Heidelberg, Germany. [5]Genome Biology Unit, European Molecular Biology Laboratory (EMBL), Heidelberg, Germany. [6]Heidelberg Pharma GmbH, Ladenburg, Germany. [7]Division of Theoretical Bioinformatics, German Cancer Research Center (DKFZ), Heidelberg, Germany. [8]Division of Biostatistics, German Cancer Research Center, Heidelberg, Germany. [9]Department of General, Visceral and Transplantation Surgery, Charité-Universitätsmedizin Berlin, Berlin, Germany. [10]Institute of Pathology, Charité-Universitätsmedizin Berlin, Berlin, Germany. [11]Institute of Pharmacy and Molecular Biotechnology, Bioquant, University of Heidelberg, Heidelberg, Germany. [12]Heidelberg Center for Personalized Oncology (DKFZ-HIPO), German Cancer Research Center, Heidelberg, Germany. [13]Department of General and Visceral Surgery, University Hospital Heidelberg, Heidelberg, Germany. [14]German Cancer Consortium (DKTK), Heidelberg, Germany. [15]Present addresses: Department of Pathology, Center for Integrated Diagnostics (CID), Massachusetts General Hospital, Boston, Massachusetts, USA (A.S.); Institute of Pathology, Technical University Munich (TUM), Munich, Germany (A.M. and W.W.); Sandoz Biopharmaceuticals, Oberhaching, Germany (C.R.); Department of General, Visceral and Transplant Surgery, Ludwig-Maximilians University, Munich, Germany (J.W.). [16]These authors contributed equally to this work. [17]These authors jointly directed this work. Correspondence should be addressed to A.T. (a.trumpp@dkfz.de) or M.R.S. (martin.sprick@hi-stem.de).

Received 6 November 2015; accepted 23 December 2015; published online 8 February 2016; doi:10.1038/nm.4038

Here we show that the exocrine-like PDAC subtype is resistant toward the small-molecule drugs dasatinib, erlotinib and paclitaxel, and that this resistance is mediated by a cell-autonomous CYP3A5-dependent drug detoxification mechanism. CYP3A5 also contributes to acquired drug resistance in other subtypes of PDAC and in other malignancies.

RESULTS

Establishment of PDAC models

First, we established patient-derived PDAC models to provide an *in vitro* and *in vivo* platform for functional studies. Patient-derived PDAC specimens were surgically grafted onto the pancreas of immune-deficient NOD.Cg-*Prkdc*^{scid}*Il2rg*^{tm1Wjl} (NSG) mice, which allow efficient human cell engraftment. Tumors from primary xenografts (PT) were then used to propagate primary PDAC cell lines referred to as PACO (pancreatic adenocarcinoma) lines (**Fig. 1a** and **Supplementary Table 1**). Comparison of the resulting PACO cell–derived tumors (DT) with the original xenografts (PT) showed conservation of histomorphological characteristics (**Fig. 1a**) and RNA expression profiles (**Supplementary Table 2**). By matching recent genomic profiling data[16–18], we found that all eight analyzed PACO lines harbored mutations in *KRAS* and that six of eight had mutations in *TP53* (**Supplementary Table 3**).

Next we determined which PDAC subtypes were represented in our PDAC models by using the PDAssigner genes[11]—a gene signature developed for classifying classical, QM-PDA and exocrine-like PDAC—and gene-set enrichment analysis (GSEA) to subtype eight PACO lines, as well as their respective PT and DT xenografts. All three subtypes, including the exocrine-like subtype, were represented (**Supplementary Fig. 1a**,**b**). Specifically, the gene expression profiles of two of our PACO lines and xenografts were enriched for the classical subtype (PACO2 and PACO17), whereas three were enriched for the exocrine-like subtype (PACO10, PACO14 and PACO18) and three for the QM-PDA subtype (PACO7, PACO9 and PACO19). Taken together, these results demonstrate that our models faithfully preserve the histomorphological characteristics of the originating tumors and, for the first time, enable the study of functional differences between all three PDAC subtypes.

Prognostic value of HNF1A and KRT81 expression

Because histopathology supplemented by immunohistochemistry is still currently the standard method for tumor subtyping, we sought to identify surrogate protein markers for each of these three PDAC subtypes to facilitate clinical patient stratification. We subjected PACO cell lines to array-based gene expression profiling. To generate a candidate biomarker list, we filtered a list of genes that were strongly (>5-fold; $P < 0.05$) differentially expressed between the different PACO subtypes for candidates that showed heterogeneous expression across PDAC specimens in the Protein Atlas database[19]. Additionally, GSEA of transcription factor activity gene sets on the original expression profiles revealed an enrichment of transcripts with binding sites for the transcription factor HNF1A in the exocrine-like subtype, suggesting HNF1A as a putative marker for this subtype (data not shown). We stained PACO lines and xenografts for all marker candidates, and

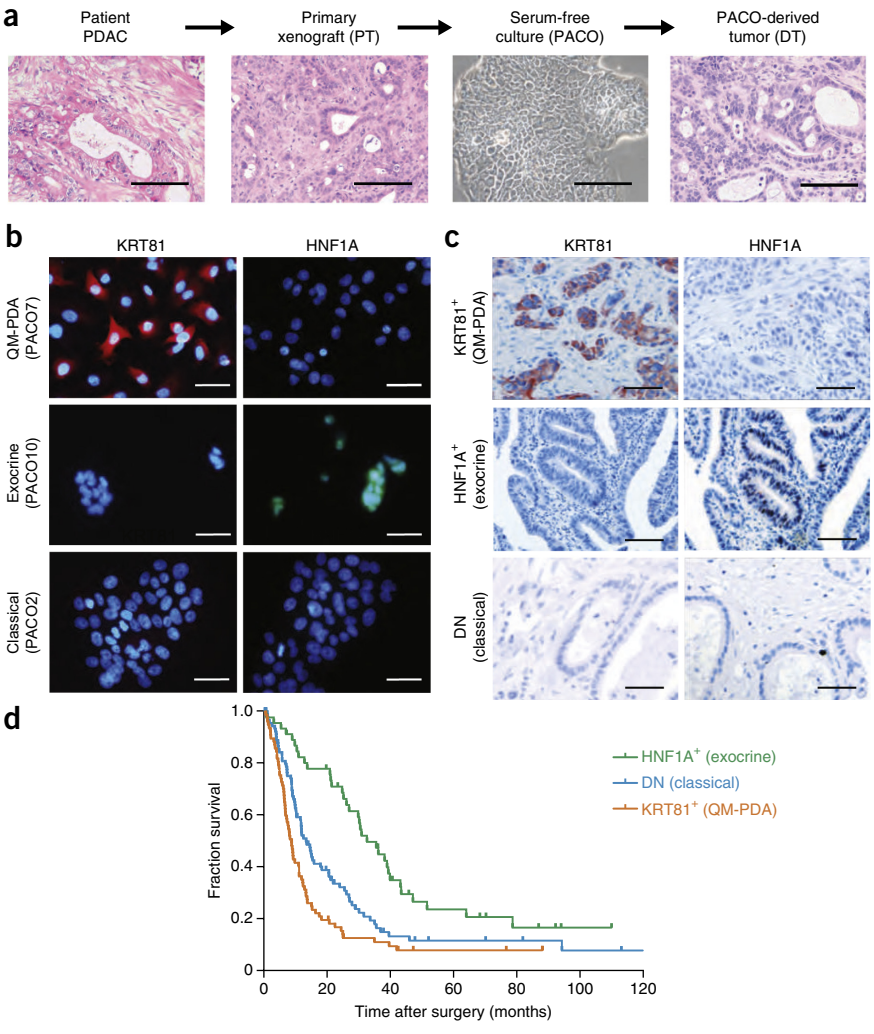

Figure 1 Subtype stratification of PDAC models and patients by using two markers. (**a**) Schematic overview of the experimental workflow used to generate orthotopic xenografts and PACO cell lines, and images showing H&E staining of a human PDAC tumor sample and the corresponding first-passage xenograft (PT), phase-contrast imaging of the derived cell line (PACO10) and H&E staining of the respective derived xenograft (DT). Scale bars, 100 µm. (**b**) Immunofluorescence staining for KRT81 (left, red) and HNF1A (right, green) in PACO lines from the QM-PDA (top), exocrine-like (exocrine; middle) and classical (bottom) PDAC subtypes ($n = 3$ per group). Nuclei are represented in blue. Scale bars, 50 µm. (**c**) KRT81- (left) and HNF1A-immunostained (right) paraffin sections from a TMA of individuals with PDAC ($n = 241$). Scale bars, 100 µm. (**d**) Kaplan-Meier analysis of overall survival of subjects with PDAC ($n = 217$). Tumor sections on the TMA were retrospectively subtyped into three groups on the basis of KRT81 and HNF1A expression, as determined by immunostaining (HNF1A$^+$ (exocrine-like), $n = 46$; DN (classical), $n = 92$; KRT81$^+$ (QM-PDA), $n = 79$). $P < 0.001$; by log-rank test.

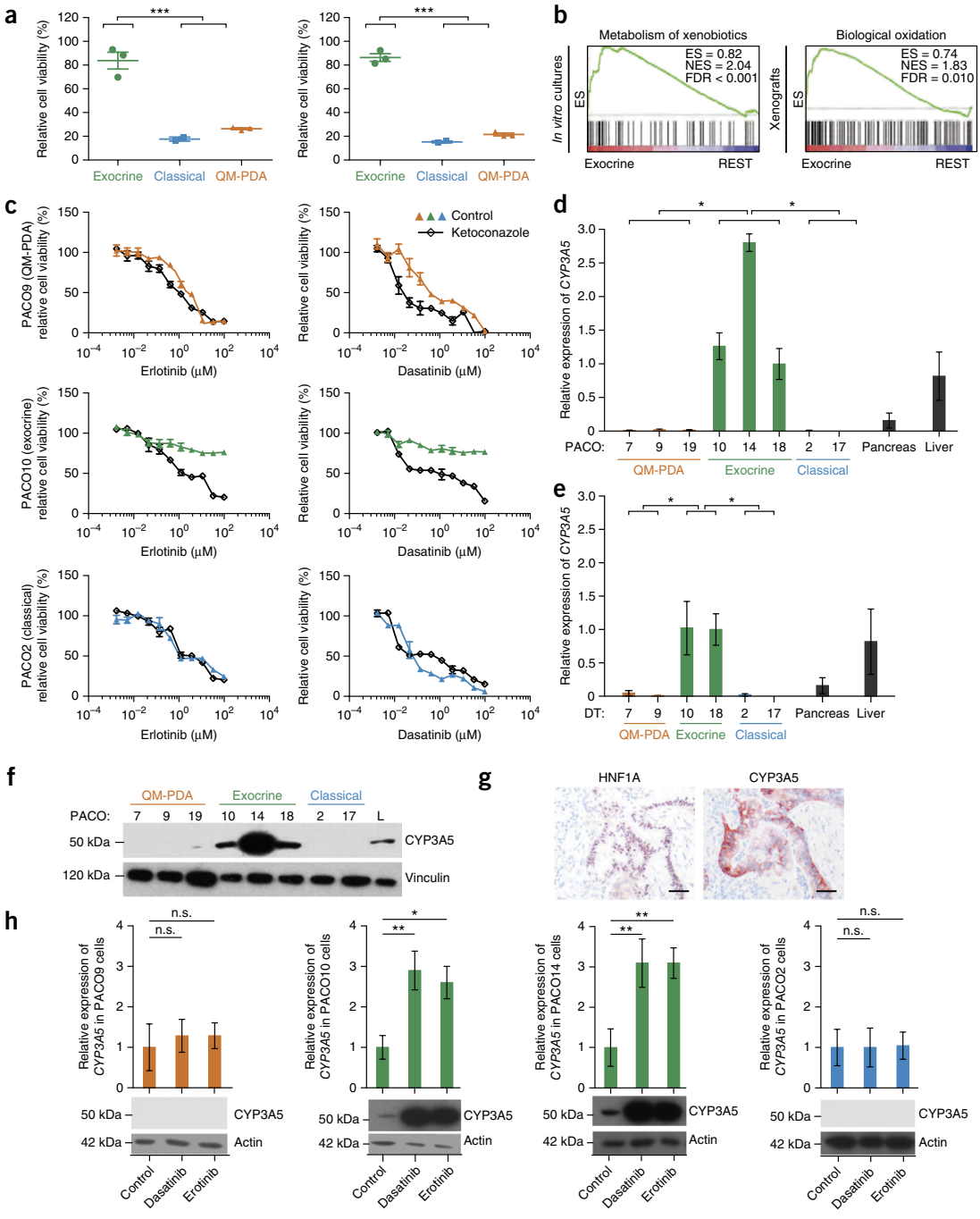

Figure 2 Exocrine-like PDAC cells, which express CYP3A5, are resistant to TKIs. (**a**) PACO line–specific drug sensitivities to 1 μM erlotinib (left) or dasatinib (right) after 48 h of treatment. Each symbol represents an individual PACO line ($n = 2$ biological replicates per PACO line). Error bars depict mean ± s.d. $^{***}P < 0.001$; by grouped one-way analysis of variance (ANOVA). (**b**) GSEA of the PACO exocrine-like PDAC cell lines (left) or xenografts (PT + DT; right) compared to the cell lines or xenografts, respectively, of the classical and QM-PDA PDAC subtypes (REST), using the indicated gene signatures. Statistical significance was assessed using 10,000 permutations. ES, enrichment score; NES, normalized enrichment score; FDR, false-discovery rate. (**c**) Sensitivity of QM-PDA (top), exocrine-like (middle) and classical (bottom) PACO lines treated with erlotinib (left) or dasatinib (right) for 48 h after pretreatment with ketoconazole (100 nM; open diamonds) or vehicle (colored triangles) for 2 h ($n = 3$ per group; one representative example of three biological replicates is shown). Error bars depict mean ± s.e.m. of technical replicates. (**d**,**e**) *CYP3A5* expression, as measured by qRT-PCR, in PACO lines (**d**) and PACO-derived xenografts (DT) (**e**), as compared to that in pancreas and liver ($n = 3$ per cell type). Values are relative to those for *CYP3A5* expression in PACO18 cells. Error bars depict mean ± s.e.m. $^{*}P < 0.05$; by grouped one-way ANOVA. (**f**) Immunoblot analysis for CYP3A5 expression in PACO cell lines. Vinculin was used as a loading control. L, liver protein lysate. (**g**) Representative images showing immunostaining for HNF1A (left) and CYP3A5 (right) in sections from individuals with HNF1A^{+} PDAC ($n = 217$). Scale bars, 100 μm. (**h**) qRT-PCR (top, graphs) and immunoblot (bottom) analyses for CYP3A5 expression before (control) and after treatment with 10 μM dasatinib or erlotinib in representative QM-PDA (PACO9), exocrine-like (PACO10 and PACO14) and classical (PACO2) PACO lines ($n = 3$ per group per condition). Actin was used as a loading control for immunoblots. For qRT-PCR data, values are relative to those of untreated controls. Error bars depict mean ± s.e.m. $^{*}P < 0.05$, $^{**}P < 0.01$; n.s., not significant; by Student's *t*-test.

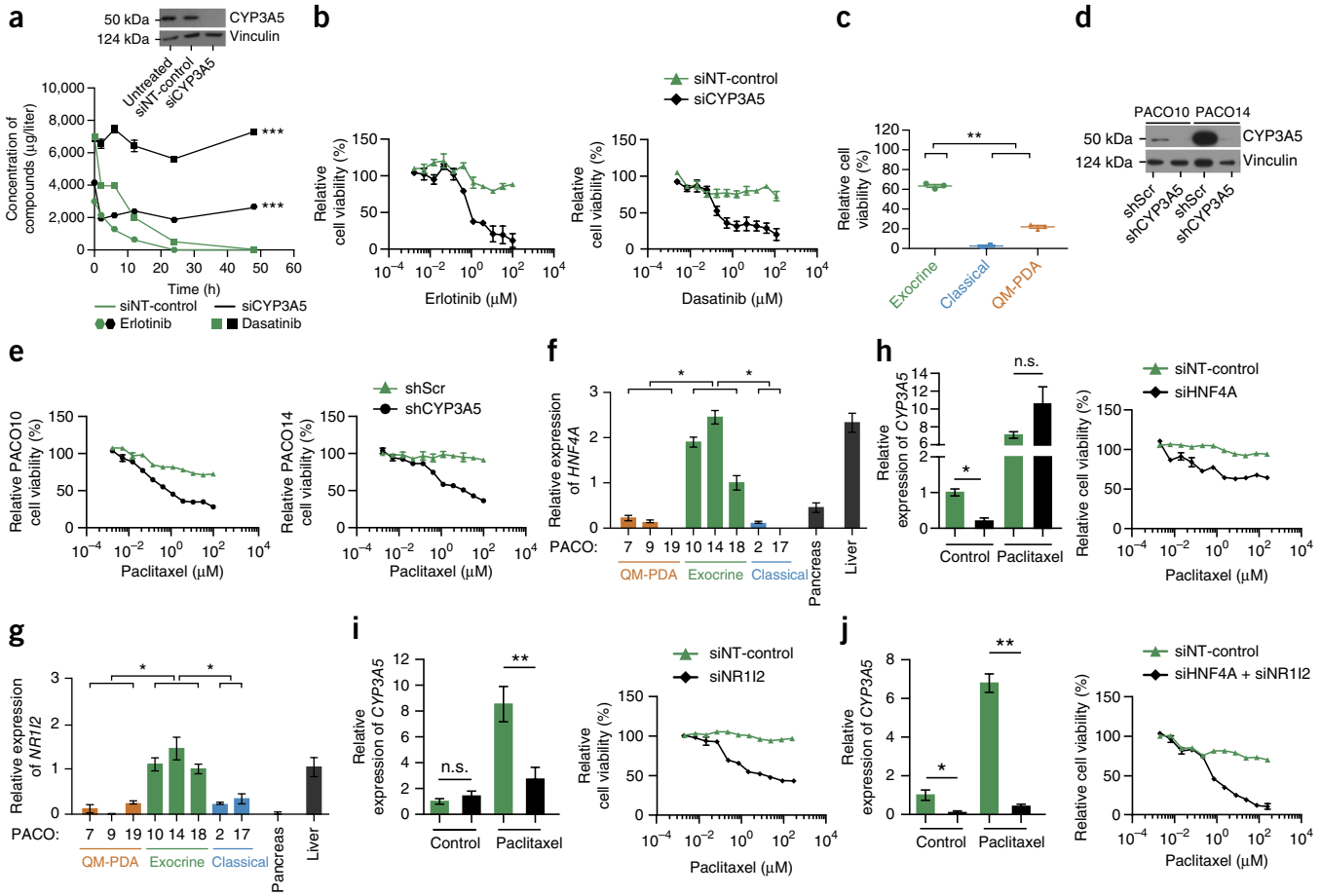

Figure 3 CYP3A5 mediates drug resistance and is regulated by *HNF4A* and *NR1I2* expression in exocrine-like PDAC cells *in vitro*. (**a**) Top, immunoblot analysis for CYP3A5 expression in untreated PACO14 exocrine-like PDAC cells or those transfected with a non-targeting (siNT-control) or *CYP3A5*-specific (siCYP3A5) siRNA. Vinculin was used as a loading control. Bottom, concentrations, as determined by LC-MS/MS analysis, of erlotinib or dasatinib in the supernatants of PACO14 cell cultures after transfection with siCYP3A5 or siNT-control and treatment with erlotinib or dasatinib (10 µM) ($n = 3$ per condition). Error bars depict mean ± s.e.m. $***P < 0.001$; by two-way ANOVA. (**b**) Sensitivity of PACO14 exocrine-like PDAC cells that were transfected with siNT-control (green) or siCYP3A5 (black) to treatment with erlotinib (left) or dasatinib (right) for 48 h ($n = 3$ per group; one representative example of three biological replicates is shown). Error bars depict mean ± s.e.m. of technical replicates. (**c**) PACO line–specific sensitivities to 1 µM paclitaxel after 48 h of treatment. Each symbol represents an individual PACO line ($n = 2$ biological replicates per PACO line). Error bars depict mean ± s.d. $**P < 0.01$; by grouped one-way ANOVA. (**d**) Immunoblot analysis for CYP3A5 in two shCYP3A5- or shScr-expressing exocrine-like PDAC lines. Vinculin was used as a loading control. (**e**) Sensitivity of shCYP3A5- or shScr-expressing PACO10 (left) and PACO14 (right) cells to treatment with paclitaxel for 48 h ($n = 3$ per group; one representative example of three biological replicates is shown). Error bars depict mean ± s.e.m. of technical replicates. (**f**,**g**) qRT-PCR analysis, normalized to mRNA levels in PACO18 cells, of *HNF4A* (**f**) and *NR1I2* (**g**) in PACO lines, pancreas and liver ($n = 3$ per cell type). Error bars depict mean ± s.e.m. $*P < 0.05$; by grouped one-way ANOVA. (**h**–**j**) *CYP3A5* expression (left, $n = 3$ per group) and drug sensitivity (right; $n = 3$ per group, one representative example is shown) of siNT-control–transfected (**h**–**j**), siHNF4A-transfected (**h**), siNR1I2-transfected (**i**), or siHNF4A- and siNR1I2-transfected (**j**) PACO14 cells after treatment with 10 µM (left) or serial dilutions (right) of paclitaxel or DMSO (control) for 48 h. mRNA expression values are relative to those from DMSO-treated, siNT-control–transfected cells. Error bars depict mean ± s.e.m. of biological replicates (left) and of technical replicates (right). $*P < 0.05$, $**P < 0.01$; n.s., not significant; by Student's *t*-test.

evaluated signal intensity and subtype specificity (**Supplementary Table 4**). We excluded markers that stained only weakly or that were not subtype specific. This analysis identified positive nuclear staining for HNF1A specifically in exocrine-like PDAC cells, whereas staining for cytokeratin 81 (KRT81) was specific for cells of the QM-PDA PDAC subtype (**Fig. 1b**). Additionally, in The Cancer Genome Atlas (TCGA) pancreatic adenocarcinoma (PAAD) cohort, *KRT81* expression also inversely correlated with that of *HNF1A* (**Supplementary Fig. 1c**). None of the candidate markers for the classical PDAC subtype showed a reliable and exclusive staining pattern in cells of this subtype. Nevertheless, the specificity of KRT81 and HNF1A staining allowed us to define classical subtype specimens as being double negative (DN) for these markers. Hence, we defined surrogate markers for the three subtypes as $KRT81^{+}HNF1A^{-}$ for the QM-PDA subtype, $KRT81^{-}HNF1A^{+}$ for the exocrine-like subtype and $KRT81^{-}HNF1A^{-}$ for the classical subtype.

We verified the association of our marker-defined subtypes with the PDAssigner signatures in an independent validation cohort of primary PDAC xenografts (**Supplementary Table 5**). Principal component analysis (PCA) demonstrated that transcriptional profiles clustered according to KRT81- and HNF1A-defined subtypes (**Supplementary Fig. 1d**). Hierarchical clustering using the PDAssigner genes further showed a separation into three groups, revealing a high concordance with our marker-defined groups (**Supplementary Fig. 1e**). GSEA

of the marker-defined groups revealed enrichment of the QM-PDA signature in the KRT81$^+$ tumors and of the exocrine-like signature in the HNF1A$^+$ tumors. The DN tumors were enriched for all three signatures and could not be unequivocally assigned (**Supplementary Fig. 1f**), suggesting that the PDAssigner signature would need to be improved for a more robust classification. Collectively, our surrogate markers separate the validation cohort into three distinct groups, of which the KRT81$^+$ and HNF1A$^+$ cases are enriched in the respective PDAssigner-defined subtypes[11].

Next we tested whether subtype stratification of a cohort of 231 individuals with PDAC, by using these two markers is associated with clinical outcome. In a retrospective study using immunohistochemistry, we designated these PDAC tumors as 45% DN, 35% KRT81$^+$ and 20% HNF1A$^+$ (**Fig. 1c**,**d** and **Supplementary Table 6**). We also identified 14 KRT81$^+$HNF1A$^+$ double-positive specimens and excluded them from the analysis. Log-rank analysis revealed significant differences in overall survival of individuals with PDAC of different subtypes ($P < 0.001$) (**Fig. 1d**). Subjects with HNF1A$^+$ tumors had the best mean survival (43.5 months), followed by those with the DN subtype (26.3 months) and the KRT81$^+$ subtype (16.5 months). Moreover, Cox proportional-hazards multivariate regression analysis revealed that the survival impact of the subtype classification is independent of established conventional prognostic factors such as stage, grade and age[20,21] (**Supplementary Table 7**). Subtype was associated with grade, as the HNF1A$^+$ cases were more differentiated (24% grade 3), the KRT81$^+$ samples tended to be less differentiated (50.6% grade 3), and the DN cases ranged in between (41.5% grade 3) (**Supplementary Table 8**). Although this association was significant ($P = 0.01$), grade alone was insufficient to predict subtype. Hence, HNF1A and KRT81 can be used to stratify patients into subtypes of PDAC that are associated with differences in overall patient survival.

Exocrine-like PDAC cells are resistant to tyrosine kinase inhibitors

To address whether the subtypes differ in drug sensitivity, PACO lines were treated with the epidermal growth factor receptor (EGFR) tyrosine kinase inhibitor (TKI) erlotinib and the SRC and ABL1 tyrosine kinase–selective TKI dasatinib, which are approved or under investigation for the treatment of PDAC, respectively[22–24]. We treated PACO lines of each subtype with 1 μM (**Fig. 2a**) or 10 μM (**Supplementary Fig. 2a**) erlotinib and dasatinib, which corresponds to 0.3- to 3-fold and 6- to 60-fold peak plasma concentrations reported in humans, respectively[25,26]. Analysis after 48 h of treatment revealed that the classical and QM-PDA cells were drug sensitive, whereas the exocrine-like cells were almost completely drug resistant. To exclude the possibility that the observed resistance was due to varying proliferation rates, we treated the PACO lines as described above for 7 d and confirmed the difference in drug response (**Supplementary Fig. 2b**,**c**). To identify the mechanisms underlying the observed drug resistance, we used GSEA to compare the exocrine-like PACO lines and xenografts with the classical and the QM-PDA PACO lines and xenografts. This analysis revealed an enrichment of signatures comprising genes involved in xenobiotic biotransformation in the exocrine-like PDAC models (**Fig. 2b** and **Supplementary Fig. 2d**,**e**). For validation we analyzed an independent data set generated from laser-microdissected PDAC[11] and confirmed the upregulation of similar gene sets in exocrine-like PDAC samples (**Supplementary Fig. 2f**). Thus, xenobiotic biotransformation might contribute to the observed drug resistance in cells of the exocrine-like PDAC subtype.

CYP family enzymes systemically metabolize small-molecule drugs by oxidation, resulting in potential inactivation of the drugs[27,28]. To test whether xenobiotic biotransformation is indeed involved in the observed drug resistance, we pretreated cells of each subtype with the pan-CYP inhibitor ketoconazole[14]. We pretreated one PACO line of each subtype with 100 nM ketoconazole or vehicle for 2 h, added serial dilutions of erlotinib or dasatinib and determined relative cell viability after 48 h. To compare TKI effects across independent experiments, we calculated activity areas as previously described[29]. Ketoconazole pretreatment significantly increased TKI sensitivity exclusively in the exocrine-like PDAC cells, rendering their drug response comparable to that in the other subtypes (**Fig. 2c** and **Supplementary Fig. 2g**). These results suggest that CYPs contribute to drug resistance in PDACs of the exocrine-like subtype.

CYP3A5 is expressed and inducible in exocrine-like PDAC cells

Members of the CYP3A subfamily are major contributors to xenobiotic biotransformation of small-molecule drugs in the liver[12].

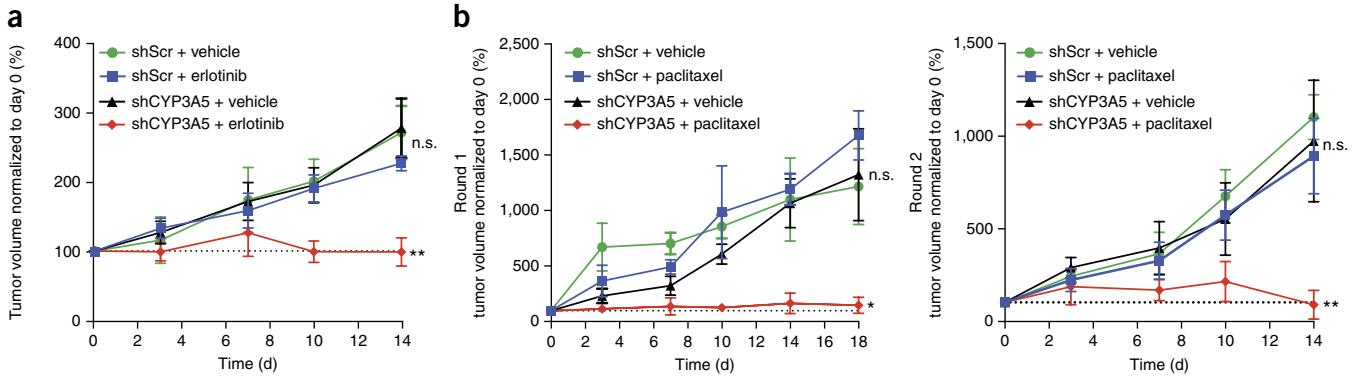

Figure 4 CYP3A5 mediates drug resistance in exocrine-like PDAC cells *in vivo*. (**a**) Growth curves of PDAC xenografts from mice with shScr- or shCYP3A5-expressing PACO14 exocrine-like cells that were treated for two cycles of 5 d with erlotinib (100 mg per kg body weight (mg/kg)) and 2 d of recovery. (**b**) Growth curves of PDAC xenografts from mice with shScr- or shCYP3A5-expressing PACO14 exocrine-like cells that were treated with two cycles of 5 d with paclitaxel (2 mg/kg) and 2 d recovery, followed by 4 d of treatment with paclitaxel (left, round 1). Cells from one xenograft per treatment group were re-injected into previously untreated mice, which were then treated for two cycles of 5 d with paclitaxel and 2 d of recovery (right, round 2) ($n = 6$ mice per treatment group). Tumor volume was measured with a digital caliper and normalized to that at baseline (day 0, dashed line). Error bars depict mean ± s.e.m. P values were determined at the end point using one-sided Mann-Whitney U test. $^*P < 0.05$; $^{**}P < 0.01$; n.s., not significant.

We thus tested expression of all three CYP3A family members—*CYP3A4*, *CYP3A5* and *CYP3A7*—in PACO cell lines and DTs. qRT-PCR analysis revealed that *CYP3A5* is exclusively expressed in the exocrine-like subtype at comparable or even higher levels than in normal liver and pancreas (**Fig. 2d**,**e**). In contrast, expression of *CYP3A4* and *CYP3A7* was low or absent (**Supplementary Fig. 2h–k**). The specific expression of *CYP3A5* in exocrine-like PDAC cells was also confirmed at the protein level in PACO lines (**Fig. 2f** and **Supplementary Fig. 2l**) and in specimens of individuals with HNF1A^{+} tumors (**Fig. 2g**). The marker-defined exocrine-like

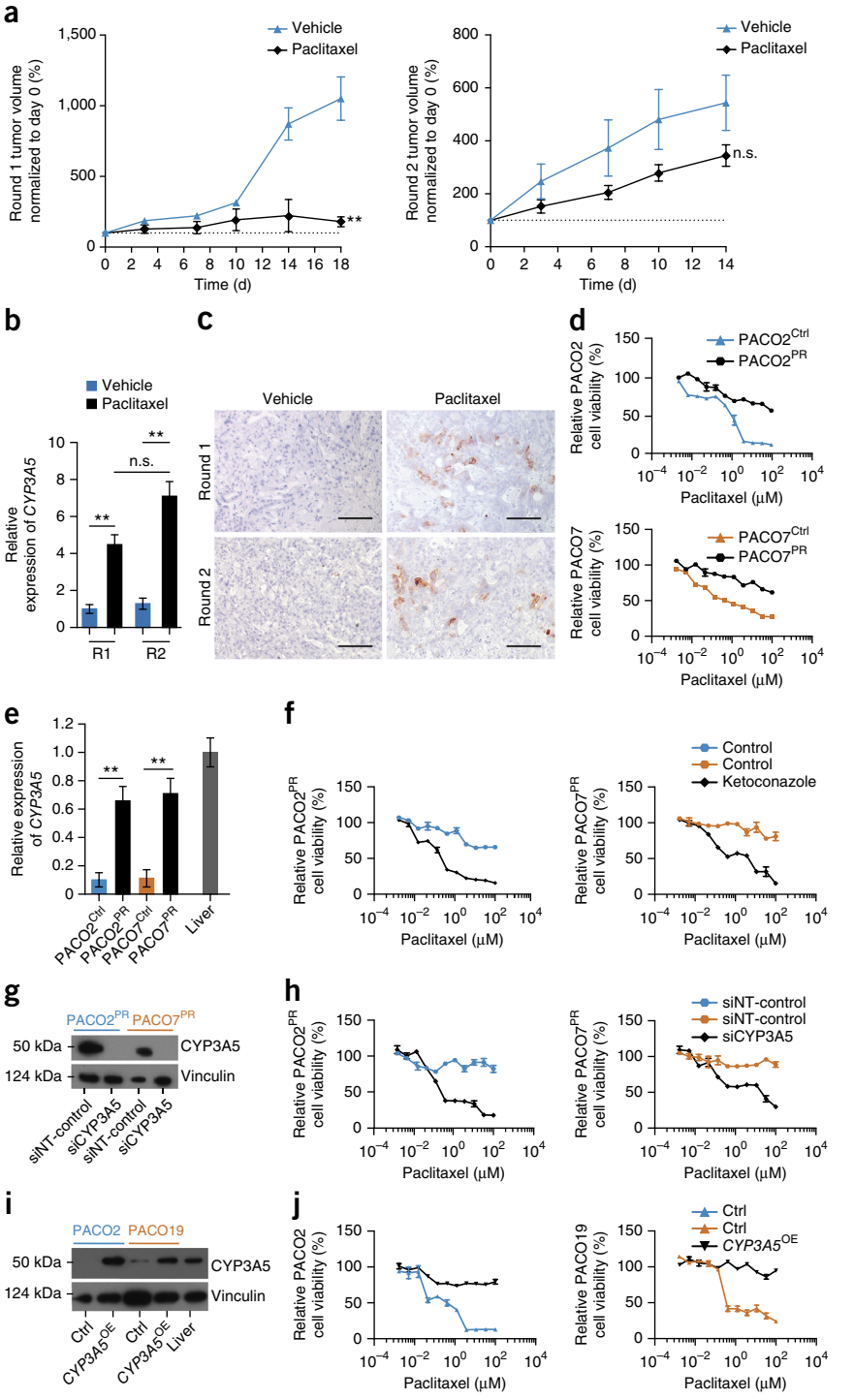

Figure 5 CYP3A5 contributes to acquired resistance in QM-PDA and classical PDAC cells. (**a**) Left, growth curves of PDAC xenografts derived from PACO17 classical PDAC cells treated as described for **Figure 4b** round 1. Right, growth curves of tumors using cells from one xenograft per group that were re-injected into previously untreated mice, which were then treated as described for **Figure 4b** round 2 ($n = 6$ mice per treatment group). Error bars depict mean ± s.e.m. P values were determined at the end point using one-sided Mann-Whitney U test. $^{**}P < 0.01$; n.s., not significant. (**b**) qRT-PCR analysis of *CYP3A5* expression in PACO17-derived round one (R1) and round two (R2) tumors after treatment with paclitaxel or vehicle ($n = 3$ mice per group). Values are relative to those of R1 tumors from vehicle-treated control mice. Error bars depict mean ± s.e.m. $^{**}P < 0.01$; n.s., not significant; by Student's t-test. (**c**) Representative images ($n = 3$) for CYP3A5 immunostaining in sections from PACO17-derived R1 (top) and R2 (bottom) xenografts after treatment of mice with vehicle (left) or paclitaxel (right). Scale bars, 100 μm. (**d**) Drug-sensitivity curves for parental (PACO2^{Ctrl} and PACO7^{Ctrl}) and paclitaxel-resistant (PACO2^{PR} and PACO7^{PR}, respectively) classical (PACO2) and QM-PDA (PACO7) cell lines treated with paclitaxel for 48 h ($n = 3$ per group; one representative example of three biological replicates is shown). Error bars depict mean ± s.e.m. of technical replicates. (**e**) qRT-PCR analysis comparing *CYP3A5* expression in PACO2^{Ctrl} and PACO7^{Ctrl} cells to that in PACO2^{PR} and PACO7^{PR} cells ($n = 3$ per group). Values are relative to those derived from liver mRNA. Error bars depict mean ± s.e.m. $^{**}P < 0.01$; by Student's t-test. (**f**) Drug-sensitivity curves for PACO2^{PR} (left) and PACO7^{PR} (right) cells treated with paclitaxel for 48 h after pretreatment with ketoconazole (100 nM) or vehicle for 2 h ($n = 3$ per group; one representative example of three biological replicates is shown). Error bars depict mean ± s.e.m. of technical replicates. (**g**) Anti-CYP3A5 immunoblot of siNT-control or siCYP3A5 transfected PACO2^{PR} and PACO7^{PR} cells. Vinculin was used as a loading control. (**h**) Drug-sensitivity curves for siNT-control- or siCYP3A5-transfected PACO2^{PR} (left) and PACO7^{PR} (right) cells treated with paclitaxel for 48 h ($n = 3$ per group; one representative example of three biological replicates is shown). Error bars depict mean ± s.e.m. of technical replicates. (**i**) Representative immunoblot analysis ($n = 3$) for CYP3A5 in classical (PACO2) and QM-PDA (PACO19) cell lines transduced with either an empty control vector (Ctrl) or one that overexpresses *CYP3A5* (CYP3A5^{OE}). Vinculin was used as a loading control. (**j**) Sensitivity of PACO2 (left) and PACO19 (right) cells transduced with a control or a *CYP3A5*-overexpressing vector to treatment with paclitaxel for 48 h ($n = 3$ per group; one representative example of three biological replicates is shown). Error bars depict mean ± s.e.m. of technical replicates.

xenografts of the validation cohort of primary PDAC xenografts also expressed significantly more *CYP3A5* than those of the other two subtypes (exocrine-like versus QM-PDA: $P = 0.0043$; exocrine-like versus classical: $P = 0.0435$) (**Supplementary Fig. 2m**). Consistent with these findings, expression of *CYP3A5* correlated positively with that of *HNF1A* and inversely with expression of *KRT81* in the PAAD data set (**Supplementary Fig. 2n**).

Enzymes involved in xenobiotic biotransformation can be induced in response to their substrates[30]. To test whether this regulatory mechanism is also functional in PDAC cells, we measured *CYP3A5* mRNA and CYP3A5 protein expression in PACO lines at steady state and in response to treatment with 10 µM dasatinib or erlotinib. Exposure to either drug boosted CYP3A5 expression in the exocrine-like, but not in the classical and QM-PDA, PACO lines (**Fig. 2h**). No increase in expression of *CYP3A4* or *CYP3A7* was observed (**Supplementary Fig. 2o**). Taken together, these data reveal that CYP3A5 is highly expressed, and that its expression can be further induced, in cells of the exocrine-like PDAC subtype *in vitro*.

CYP3A5 mediates drug resistance in exocrine-like PDAC cells

To test whether CYP3A5 metabolizes erlotinib and dasatinib in exocrine-like PDAC cells, we measured the chemical modification of these drugs in two different exocrine-like PACO lines that were transfected with either a *CYP3A5*-specific (siCYP3A5) or a non-targeting (siNT-control) short interfering RNA (siRNA). Quantitative mass spectrometric analysis (using liquid chromatography–coupled tandem mass spectrometry (LC-MS/MS))[27,28] revealed a rapid conversion of erlotinib and dasatinib in siNT-control–transfected cells, as illustrated by loss of their unmodified forms from the supernatant; this did not occur in cells transfected with the siCYP3A5 (**Fig. 3a** and **Supplementary Fig. 3a**,**b**). Chemical modifications by CYP enzymes can have a neutral effect, or they can activate or inactivate small-molecule inhibitors[31]. If CYP3A5 inactivates these compounds, its expression would explain the observed resistance to erlotinib and dasatinib in exocrine-like PDAC cells. Indeed, siRNA-mediated knockdown of *CYP3A5* significantly and exclusively sensitized the exocrine-like PACO cells to these drugs (**Fig. 3b** and **Supplementary Fig. 3c**,**d**). As microtubule-targeting taxanes are also substrates for CYP3A family members[32,33], we next asked whether *CYP3A5* expression affects the recently introduced paclitaxel-based treatment for PDAC[5,6]. Treatment of PACO lines with paclitaxel indeed revealed that the exocrine-like PDAC subtype was significantly more resistant than the other two subtypes (**Fig. 3c** and **Supplementary Fig. 3e**–**g**). To verify the role of CYP3A5 in this context, we established exocrine-like PACO lines that stably expressed control (shScr) or *CYP3A5*-specific (shCYP3A5) shRNAs (**Fig. 3d**). Similarly to that of erlotinib and dasatinib (**Supplementary Fig. 3h**,**i**), knockdown of *CYP3A5* sensitized the exocrine-like PACO cells to paclitaxel (**Fig. 3e**).

The strong upregulation of *CYP3A5* in response to erlotinib, dasatinib and paclitaxel (**Fig. 2h** and **Supplementary Fig. 3j**) suggests a major contribution of *CYP3A5* induction to the observed drug resistance. Of the genes that encode transcription factors known to regulate the expression of CYP3A family members[34–37], *HNF4A* and *NR1I2* (also called *PXR*) are selectively expressed in exocrine-like PACO cells at levels comparable to those in normal liver (**Fig. 3f**,**g**). Whereas HNF4A-dependent transcription is activated by its ubiquitous ligand linoleic acid[38], NR1I2 initiates transcription in response to xenobiotics such as erlotinib, dasatinib and paclitaxel[39,40]. We performed individual or combined siRNA knockdowns for *HNF4A* (using siHNF4A) and *NR1I2* (using siNR1I2) to test their contribution to basal and induced expression of *CYP3A5* (**Supplementary Fig. 3k**). Basal expression of *CYP3A5* was significantly reduced by knockdown of *HNF4A* but not *NR1I2* (**Fig. 3h**,**i** and **Supplementary Fig. 3l**,**m**). In contrast, induction of *CYP3A5* expression after treatment with erlotinib, dasatinib and paclitaxel was significantly impaired by knockdown of *NR1I2* but not *HNF4A* (**Fig. 3h**,**i** and **Supplementary Fig. 3l**,**m**). Combined knockdown of *HNF4A* and *NR1I2* significantly decreased both basal and drug-induced *CYP3A5* expression (**Fig. 3j** and **Supplementary Fig. 3n**,**o**). Next, we tested the contribution of both factors to drug resistance. Knockdown of either *HNF4A* or *NR1I2* rendered exocrine-like PACO cells susceptible to all of the drugs tested (**Fig. 3h**,**i** and **Supplementary Fig. 3l**,**m**). The combined knockdown of *HNF4A* and *NR1I2* rendered the cells even more sensitive to drug treatment than that achieved by the knockdown of *HNF4A* or *NR1I2* alone (**Fig. 3j** and **Supplementary Fig. 3n**).

We next asked whether ablation of *CYP3A5* expression could sensitize established tumors to small-molecule drugs *in vivo*. We thus established subcutaneous tumors from shScr- or shCYP3A5-expressing exocrine-like PACO cells in NSG mice. After the tumors reached an average volume of 200 mm^3, the mice were treated with

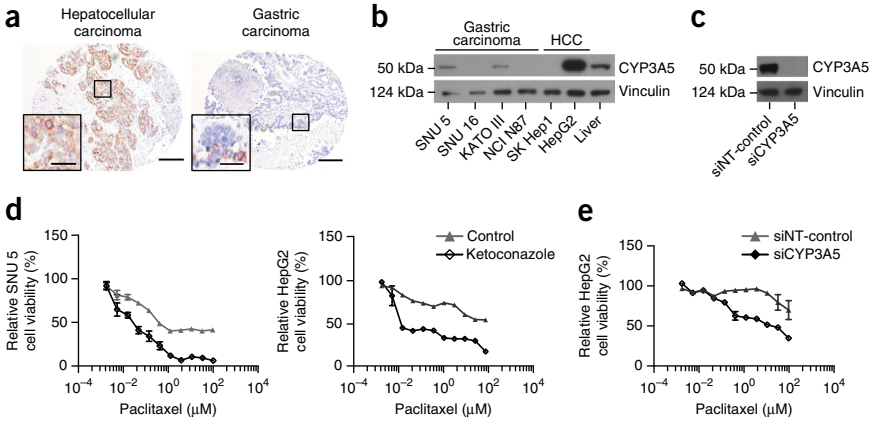

Figure 6 CYP3A5 contributes to drug resistance in other malignancies. (**a**) Representative images of CYP3A5 immunostaining of paraffin sections of human hepatocellular (left) and gastric (right) carcinoma samples from a tissue microarray consisting of samples from various tumor types ($n = 16$ per entity). Inset shows magnified image of boxed area. Scale bars, 100 µm and 5 µm (insets). (**b**) Representative immunoblot analysis ($n = 3$) comparing CYP3A5 expression in normal liver lysate with that in four gastric and two hepatocellular (HCC) carcinoma cell lines. Vinculin was used as a loading control. (**c**) Representative immunoblot analysis ($n = 3$) for CYP3A5 expression in siCYP3A5- or siNT-control–transfected HepG2 cells. Vinculin was used as a loading control. (**d**) Sensitivity of vehicle- or ketoconazole-treated (100 nM) SNU 5 (left) and HepG2 (right) cells to treatment with paclitaxel for 48 h ($n = 3$ per group; one representative example is shown). Error bars depict mean ± s.e.m. of technical replicates. (**e**) Sensitivity of siCYP3A5- or siNT-control-transfected HepG2 cells to treatment with paclitaxel for 48 h ($n = 3$ per group; one representative example of three biological replicates is shown). Error bars depict mean ± s.e.m. of technical replicates.

erlotinib or vehicle by oral gavage for five consecutive days followed by 2 d of rest, for a total of 14 d. Whereas treatment with erlotinib had no significant effect on the growth rate of the shScr-expressing tumors, growth of the shCYP3A5-expressing tumors was significantly inhibited (**Fig. 4a** and **Supplementary Fig. 4a**). Additionally, *CYP3A5* expression was significantly (PACO10: $P < 0.05$; PACO14: $P < 0.01$) increased in shScr-expressing tumors after treatment of mice with erlotinib but not vehicle (**Supplementary Fig. 4b**). Knockdown of *CYP3A5* also significantly enhanced the response to paclitaxel treatment (**Fig. 4b** and **Supplementary Fig. 4c**). To extend the *in vivo* treatment period, we re-injected cells recovered after treatment round one into secondary mice (round two). Even in round two, paclitaxel treatment significantly suppressed the growth of shCYP3A5-expressing tumors (**Fig. 4b** and **Supplementary Fig. 4c**), and *CYP3A5* expression was significantly ($P < 0.01$) higher in shScr-expressing tumors from paclitaxel-treated mice as compared to those from vehicle-treated mice (**Supplementary Fig. 4d**). We conclude that long-term suppression of *CYP3A5* expression in exocrine-like xenografts does not lead to induction of alternative resistance pathways.

CYP3A5 contributes to acquired resistance in QM-PDA and classical PDAC cells

The development of secondary resistance limits the efficacy of drug treatment in PDAC[1]. We thus asked whether CYP3A5 also contributes to acquired resistance. To this end, tumors of the classical subtype were treated with paclitaxel for two rounds for a total of 32 d. Paclitaxel treatment significantly inhibited tumor growth of classical xenografts during the first round of treatment, whereas longer-term treatment led to a marked development of paclitaxel resistance (**Fig. 5a**). *CYP3A5* mRNA and CYP3A protein expression substantially increased after paclitaxel treatment (**Fig. 5b**,**c**). Because we could not detect expression of *CYP3A4* and *CYP3A7* (**Supplementary Fig. 5a**), these data suggest a role for CYP3A5 in acquired drug resistance.

To functionally explore this hypothesis, we generated paclitaxel-resistant classical ($PACO2^{PR}$) and QM-PDA ($PACO7^{PR}$) PACO lines (**Fig. 5d**). Consistent with the findings from the *in vivo* drug-treatment experiments, we found that *CYP3A5* expression was significantly increased in the paclitaxel-resistant PACO sublines as compared to that in the control parental lines (**Fig. 5e**), whereas *CYP3A4* and *CYP3A7* expression was undetectable (**Supplementary Fig. 5b**). Similar results were obtained for dasatinib- and erlotininb-resistant lines (**Supplementary Fig. 5c**,**d**). Inhibition of CYP3A5 by using ketoconazole (**Fig. 5f**) or by *CYP3A5* knockdown (**Fig. 5g**,**h**) restored drug sensitivity in the paclitaxel-resistant sublines to levels comparable to that of the parental lines. Furthermore, ectopic expression of CYP3A5 in non–exocrine-like cells conferred drug resistance (**Fig. 5i**,**j** and **Supplementary Fig. 5e**,**f**), confirming that CYP3A5 upregulation is a primary mechanism responsible for the observed acquired resistance.

CYP3A5 contributes to drug resistance in other malignancies

Expression of CYP family members has been described in a range of tumors[14,41]. To address whether CYP3A5 mediates resistance in tumor types other than PDAC, we stained a tissue microarray (TMA) comprising 438 individual tissue samples from 33 distinct tumor types for CYP3A5 (**Fig. 6a** and **Supplementary Fig. 6a**). Samples from 10 of 33 tumor types expressed detectable amounts of CYP3A5. We found particularly high expression of CYP3A5 in the majority of hepatocellular carcinoma, gastric carcinoma, cervical carcinoma, adrenal gland cortical carcinoma and biliary tract cancer tissue samples, indicating that CYP3A5 may mediate drug resistance in a considerable fraction of solid tumors (**Supplementary Table 9**). To begin to test this hypothesis, we screened a number of gastric and hepatocellular carcinoma cell lines for CYP3A5 expression. The gastric cancer cell line SNU 5 and the hepatocellular carcinoma cell line HepG2 expressed CYP3A5 at levels comparable to those in normal liver and were selected for further experiments (**Fig. 6b** and **Supplementary Fig. 6b**). We found that paclitaxel exposure resulted in the induction of *CYP3A5* expression in these cell lines (**Supplementary Fig. 6c**) and that pretreatment with ketoconazole sensitized both cell lines to paclitaxel treatment (**Fig. 6d**). We observed a similar sensitization after *CYP3A5* knockdown in HepG2 cells (**Fig. 6c**,**e** and **Supplementary Fig. 6d**), suggesting that CYP3A5 expression contributes to drug resistance in tumor types other than PDAC.

DISCUSSION

Here we confirm the existence of three reported PDAC subtypes[11] and identify two surrogate markers, HNF1A and KRT81, for tumor stratification by using immunohistochemistry. Our finding—that individuals with resectable $HNF1A^{+}$ exocrine-like PDAC have the best survival rates—might be perceived contradictory at first. However, patient survival is not only determined by drug response; growth rate of the primary tumor as well as the propensity for, and the pattern of, metastasis also influence survival[38]. In fact, exocrine-like PACO cells are slower to expand in culture and have a delayed onset in xenograft formation as compared to PACO cells of the classical and QM-PDA subtypes (data not shown). This suggests that tumors originating from exocrine-like PDAC cells are the least aggressive PDAC subtype, despite their resistance to drug treatments.

Drug response in cancer patients is influenced by hepatic CYPs that mediate systemic drug metabolism, whereas only minor amounts of these enzymes are expressed in other tissues[42,43]. Although a role for CYPs in tumor cell–autonomous drug detoxification has been postulated[34,44–55], this concept has never been functionally demonstrated. We now demonstrate that CYP3A5 contributes to both basal and acquired resistance to small-molecule drugs in PDAC. Because CYP3A5 is dispensable for normal physiology[56,57], its inhibition in cancers is a promising therapeutic option. It may be challenging to design a CYP3A5-specific inhibitor owing to the structural similarities between CYP3A family members, although a highly selective CYP3A4 inhibitor has been reported[58]. Expression of CYP family enzymes are frequently induced by their substrates[12,37]. We show that basal and substrate-induced expression of CYP3A5 is differentially regulated by HNF4A and NR1I2. Interfering with these regulatory mechanisms may provide an alternative approach to suppress the CYP3A5 pathway, thus overcoming basal and acquired drug resistance in PDAC.

The described CYP3A5-mediated resistance mechanism is not limited to PDAC, as expression and functional analyses suggest that subsets of other cancer types may use the same resistance strategy. Consequently, *CYP3A5* expression should be taken into consideration in the interpretation of results from drug trials, as targets of this enzyme probably have decreased efficacy in CYP3A5-expressing tumors.

METHODS

Methods and any associated references are available in the online version of the paper.

Accession codes. Microarray data are available in the ArrayExpress database (http://www.ebi.ac.uk/arrayexpress) under accession number E-MTAB-4029.

Note: Any Supplementary Information and Source Data files are available in the online version of the paper.

ACKNOWLEDGMENTS

We thank E. Soyka, S. Bauer and A. Hieronymus for excellent technical assistance. We also thank the microarray and the next-generation sequencing (NGS) unit of the Genomics and Proteomics Core Facility, DKFZ, for providing expression profiling, NGS and related services, and all members of the flow cytometry core facility for excellent support. We thank DKFZ-HIPO for technical support and funding through grant no. HIPO-015 (M.S., R.E., N.A.G., O.S., T.H., A.T. and M.R.S.). This work was supported in part by the Dietmar Hopp Foundation and the BioRN Spitzencluster 'Molecular- and Cell-based Medicine' (E.M.N., C.E., E.E., C.K., V.V., W.N., C.R., J.E., F.M.Z., A.T. and M.R.S.), the German Bundesministerium für Bildung und Forschung (BMBF) e:Med program for systems biology (PANC-STRAT consortium, grant no. 01ZX1305; A.T., M.R.S., M.S., R.E., N.A.G., T.H., O.S., A.S., A.M. and W.W.), the Helmholtz Preclinical Comprehensive Cancer Center (E.E., A.T. and M.R.S.) and the DKFZ-NCT program NCT3.0 (A.T., M.R.S., O.E., M.S., R.E., N.A.G., T.H. and O.S.). A.S. was supported by a fellowship from the NCT–Heidelberg School of Oncology (HSO). E.E. is recipient of an EMBO long-term fellowship (ALTF 344-2013). The collection and processing of the specimens via PancoBank was supported by Heidelberger Stiftung Chirurgie (M.W.B.), BMBF (grant no. 01GS08114; M.W.B.) and Biomaterial Bank Heidelberg–BMBH (BMBF grant no. 01EY1101; A.S. and W.W.).

AUTHOR CONTRIBUTIONS

E.M.N. and C.E. share first authorship, and A.S. and E.E. share second authorship of this paper. E.M.N. and C.E. established, conducted and analyzed the experiments; A.S., A.M. and W.W. performed immunohistological analyses of all of the tissue specimens presented and performed respective data analyses; E.E. did the immunofluorescence staining experiments and analyses on publicly available data sets; B.K., W.N. and C.R. performed RNA expression analyses on the PDAC validation cohort; C.K., V.V., J.E., F.M.Z., O.E., M.S. and R.E. provided technical and experimental support; C.L. and M.K. conducted and analyzed LC-MS/MS experiments; X.J. and A.K.-S. performed activity area calculations; P.N., M.B. and B.V.S. provided PDAC tissue microarray characterization; N.A.G., T.H., O.S., J.W. and M.W.B. provided samples of individuals with PDAC; A.T. and M.R.S. supervised the project; E.N., C.E., A.T. and M.R.S. developed the concept, designed experimental studies, analyzed the data and wrote the manuscript.

COMPETING FINANCIAL INTERESTS

The authors declare no competing financial interests.

1. Hidalgo, M. Pancreatic cancer. *N. Engl. J. Med.* **362**, 1605–1617 (2010).
2. Malvezzi, M., Bertuccio, P., Levi, F., La Vecchia, C. & Negri, E. European cancer mortality predictions for the year 2014. *Ann. Oncol.* **25**, 1650–1656 (2014).
3. Siegel, R.L., Miller, K.D. & Jemal, A. Cancer statistics, 2015. *CA Cancer J. Clin.* **65**, 5–29 (2015).
4. Burris, H.A. III *et al.* Improvements in survival and clinical benefit with gemcitabine as first-line therapy for patients with advanced pancreas cancer: a randomized trial. *J. Clin. Oncol.* **15**, 2403–2413 (1997).
5. Conroy, T. *et al.* FOLFIRINOX versus gemcitabine for metastatic pancreatic cancer. *N. Engl. J. Med.* **364**, 1817–1825 (2011).
6. Von Hoff, D.D. *et al.* Increased survival in pancreatic cancer with nab-paclitaxel plus gemcitabine. *N. Engl. J. Med.* **369**, 1691–1703 (2013).
7. Vincent, A., Herman, J., Schulick, R., Hruban, R.H. & Goggins, M. Pancreatic cancer. *Lancet* **378**, 607–620 (2011).
8. Moore, M.J. *et al.* Erlotinib plus gemcitabine compared with gemcitabine alone in patients with advanced pancreatic cancer: a phase 3 trial of the National Cancer Institute of Canada clinical trials group. *J. Clin. Oncol.* **25**, 1960–1966 (2007).
9. Biankin, A.V. & Maitra, A. Subtyping pancreatic cancer. *Cancer Cell* **28**, 411–413 (2015).
10. Kim, S. *et al.* Identifying molecular subtypes related to clinicopathologic factors in pancreatic cancer. *Biomed. Eng. Online* **13**, S5 (2014).
11. Collisson, E.A. *et al.* Subtypes of pancreatic ductal adenocarcinoma and their differing responses to therapy. *Nat. Med.* **17**, 500–503 (2011).
12. Guengrich, F.P. in *Comprehensive Toxicology* 2nd edn. (ed. McQueen, C.A.) 9.43–9.76 (Elsevier Ltd., Oxford, 2010).
13. Rochat, B. Role of cytochrome P450 activity in the fate of anticancer agents and in drug resistance: focus on tamoxifen, paclitaxel and imatinib metabolism. *Clin. Pharmacokinet.* **44**, 349–366 (2005).
14. Bruno, R.D. & Njar, V.C.O. Targeting cytochrome P450 enzymes: a new approach in anticancer drug development. *Bioorg. Med. Chem.* **15**, 5047–5060 (2007).
15. Michael, M. & Doherty, M.M. Drug metabolism by tumors: its nature, relevance and therapeutic implications. *Expert Opin. Drug Metab. Toxicol.* **3**, 783–803 (2007).
16. Yachida, S. & Iacobuzio-Donahue, C.A. Evolution and dynamics of pancreatic cancer progression. *Oncogene* **32**, 5253–5260 (2013).
17. Biankin, A.V. *et al.* Pancreatic cancer genomes reveal aberrations in axon-guidance pathway genes. *Nature* **491**, 399–405 (2012).
18. Jones, S. *et al.* Core signaling pathways in human pancreatic cancers revealed by global genomic analyses. *Science* **321**, 1801–1806 (2008).
19. Uhlen, M. *et al.* Toward a knowledge-based Human Protein Atlas. *Nat. Biotechnol.* **28**, 1248–1250 (2010).
20. Wolfgang, C.L. *et al.* Recent progress in pancreatic cancer. *CA Cancer J. Clin.* **63**, 318–348 (2013).
21. Hruban, R.H., Pitman, M.B. & Klimstra, D.S. *Tumors of the Pancreas* 6th edn. (American Registry of Pathology, Washington, D.C., 2007).
22. Hong, D.S. *et al.* A phase 1 study of gemcitabine combined with dasatinib in patients with advanced solid tumors. *Invest. New Drugs* **31**, 918–926 (2013).
23. George, T.J. Jr., Trevino, J.G. & Liu, C. Src inhibition is still a relevant target in pancreatic cancer. *Oncologist* **19**, 211 (2014).
24. Trevino, J.G. *et al.* Inhibition of *SRC* expression and activity inhibits tumor progression and metastasis of human pancreatic adenocarcinoma cells in an orthotopic nude mouse model. *Am. J. Pathol.* **168**, 962–972 (2006).
25. Ling, J. *et al.* Metabolism and excretion of erlotinib, a small-molecule inhibitor of epidermal growth factor receptor tyrosine kinase, in healthy male volunteers. *Drug Metab. Dispos.* **34**, 420–426 (2006).
26. Christopher, L.J. *et al.* Metabolism and disposition of dasatinib after oral administration to humans. *Drug Metab. Dispos.* **36**, 1357–1364 (2008).
27. Li, J., Zhao, M., He, P., Hidalgo, M. & Baker, S.D. Differential metabolism of gefitinib and erlotinib by human cytochrome P450 enzymes. *Clin. Cancer Res.* **13**, 3731–3737 (2007).
28. Wang, L. *et al.* Identification of the human enzymes involved in the oxidative metabolism of dasatinib: an effective approach for determining metabolite formation kinetics. *Drug Metab. Dispos.* **36**, 1828–1839 (2008).
29. Barretina, J. *et al.* The Cancer Cell Line Encyclopedia enables predictive modeling of anticancer drug sensitivity. *Nature* **483**, 603–607 (2012).
30. Ding, X. & Zhang, Q.Y. in *Comprehensive Toxicology* 2nd edn. (ed. McQueen, C.A.) 4.9–4.29 (Elsevier, Oxford, 2010).
31. Jänne, P.A., Gray, N. & Settleman, J. Factors underlying sensitivity of cancers to small-molecule kinase inhibitors. *Nat. Rev. Drug Discov.* **8**, 709–723 (2009).
32. Haaz, M.C., Rivory, L., Riché, C., Vernillet, L. & Robert, J. Metabolism of irinotecan (CPT-11) by human hepatic microsomes: participation of cytochrome P450 3A and drug interactions. *Cancer Res.* **58**, 468–472 (1998).
33. Sonnichsen, D.S. & Relling, M.V. Clinical pharmacokinetics of paclitaxel. *Clin. Pharmacokinet.* **27**, 256–269 (1994).
34. Burk, O. *et al.* The induction of cytochrome P450 3A5 (CYP3A5) in the human liver and intestine is mediated by the xenobiotic sensors pregnane X receptor (PXR) and constitutively activated receptor (CAR). *J. Biol. Chem.* **279**, 38379–38385 (2004).
35. Burk, O. & Wojnowski, L. Cytochrome P450 3A and their regulation. *Naunyn Schmiedebergs Arch. Pharmacol.* **369**, 105–124 (2004).
36. Tirona, R.G. *et al.* The orphan nuclear receptor HNF-4α determines PXR- and CAR-mediated xenobiotic induction of CYP3A4. *Nat. Med.* **9**, 220–224 (2003).
37. Tompkins, L.M. & Wallace, A.D. Mechanisms of cytochrome P450 induction. *J. Biochem. Mol. Toxicol.* **21**, 176–181 (2007).
38. Yuan, X. *et al.* Identification of an endogenous ligand bound to a native orphan nuclear receptor. *PLoS One* **4**, e5609 (2009).
39. Koutsounas, I., Theocharis, S., Patsouris, E. & Giaginis, C. Pregnane X receptor (PXR) at the crossroads of human metabolism and disease. *Curr. Drug Metab.* **14**, 341–350 (2013).
40. Wu, B., Li, S. & Dong, D. 3D structures and ligand specificities of nuclear xenobiotic receptors CAR, PXR and VDR. *Drug Discov. Today* **18**, 574–581 (2013).
41. Michael, M. & Doherty, M.M. Tumoral drug metabolism: overview and its implications for cancer therapy. *J. Clin. Oncol.* **23**, 205–229 (2005).
42. Pavek, P. & Dvorak, Z. Xenobiotic-induced transcriptional regulation of xenobiotic-metabolizing enzymes of the cytochrome P450 superfamily in human extrahepatic tissues. *Curr. Drug Metab.* **9**, 129–143 (2008).
43. Ding, X. & Kaminsky, L.S. Human extrahepatic cytochromes P450: function in xenobiotic metabolism and tissue-selective chemical toxicity in the respiratory and gastrointestinal tracts. *Annu. Rev. Pharmacol. Toxicol.* **43**, 149–173 (2003).
44. Downie, D. *et al.* Profiling cytochrome P450 expression in ovarian cancer: identification of prognostic markers. *Clin. Cancer Res.* **11**, 7369–7375 (2005).
45. Hukkanen, J. *et al.* Induction and regulation of xenobiotic-metabolizing cytochrome P450s in the human A549 lung adenocarcinoma cell line. *Am. J. Respir. Cell Mol. Biol.* **22**, 360–366 (2000).
46. Murray, G.I., Patimalla, S., Stewart, K.N., Miller, I.D. & Heys, S.D. Profiling the expression of cytochrome P450 in breast cancer. *Histopathology* **57**, 202–211 (2010).
47. Bergheim, I. *et al.* Cytochrome P450 levels are altered in patients with esophageal squamous-cell carcinoma. *World J. Gastroenterol.* **13**, 997–1002 (2007).
48. Dhaini, H.R. *et al.* Cytochrome P450 CYP3A4/5 expression as a biomarker of outcome in osteosarcoma. *J. Clin. Oncol.* **21**, 2481–2485 (2003).
49. Gharavi, N. & El-Kadi, A.O.S. Expression of cytochrome P450 in lung tumor. *Curr. Drug Metab.* **5**, 203–210 (2004).
50. McFadyen, M.C., Melvin, W.T. & Murray, G.I. Cytochrome P450 CYP1B1 activity in renal cell carcinoma. *Br. J. Cancer* **91**, 966–971 (2004).
51. Oyama, T. *et al.* Expression of cytochrome P450 in tumor tissues and its association with cancer development. *Front. Biosci.* **9**, 1967–1976 (2004).

52. Oyama, T. *et al.* Cytochrome P450 in non-small-cell lung cancer related to exogenous chemical metabolism. *Front. Biosci. (Schol. Ed.)* **4**, 1539–1546 (2012).
53. Schmidt, R. *et al.* CYP3A4, CYP2C9 and CYP2B6 expression and ifosfamide turnover in breast cancer tissue microsomes. *Br. J. Cancer* **90**, 911–916 (2004).
54. Sugawara, M. *et al.* Expressions of cytochrome P450, UDP-glucuronosyltranferase and transporter genes in monolayer carcinoma cells change in subcutaneous tumors grown as xenografts in immunodeficient nude mice. *Drug Metab. Dispos.* **38**, 526–533 (2010).
55. Basseville, A. *et al.* Irinotecan induces steroid and xenobiotic receptor (SXR) signaling to detoxification pathway in colon cancer cells. *Mol. Cancer* **10**, 80 (2011).
56. Kuehl, P. *et al.* Sequence diversity in *CYP3A* promoters and characterization of the genetic basis of polymorphic *CYP3A5* expression. *Nat. Genet.* **27**, 383–391 (2001).
57. Westlind-Johnsson, A. *et al.* Comparative analysis of *CYP3A* expression in human liver suggests only a minor role for CYP3A5 in drug metabolism. *Drug Metab. Dispos.* **31**, 755–761 (2003).
58. Walsky, R.L. *et al.* Selective mechanism-based inactivation of CYP3A4 by CYP3cide (PF-04981517) and its utility as an *in vitro* tool for delineating the relative roles of CYP3A4 versus CYP3A5 in the metabolism of drugs. *Drug Metab. Dispos.* **40**, 1686–1697 (2012).

ONLINE METHODS

Human tissue specimens. Tissue samples were obtained from patients admitted to the Department of General, Visceral and Transplantation Surgery, University of Heidelberg (by M.W.B.). The study was approved by the ethical committee of the University of Heidelberg (case number 301/2001) and conducted in accordance with the Helsinki Declaration; written informed consent was obtained from all patients. Patient and tumor characteristics are summarized in **Supplementary Table 1**. The PDAC validation cohort consists of a subset of the HIPO-015 study, for which xenografts were readily available. The xenografts were also derived from surgically removed specimens from individuals with PDAC that received partial pancreatoduodenectomy at the University Hospital Heidelberg. The study was approved by the ethical committee of the University of Heidelberg (case number S-206/2011) and conducted in accordance with the Helsinki Declaration; written informed consent was obtained from all patients. Patient and tumor characteristics of the PDAC xenograft validation cohort are summarized in **Supplementary Table 5**.

Xenografts of primary tumor specimens and PACO cell lines. To establish primary xenografts, tumors were cut into 1–2 mm^3 pieces and implanted onto the pancreas of 8- to 12-week-old female NOD.Cg-*Prkdc*^{scid}*Il2rg*^{tm1Wjl} (NSG) mice, which were bred in the animal facility of the German Cancer Research Center. For the generation of xenografts from the PACO lines, a suspension of 10^5–10^6 cultured cells in Matrigel (2 mg/ml) (BD) was injected into the pancreas of NSG mice. Engraftment of tumors and subsequent growth was monitored by regular palpation of the implantation site. Orthotopically grafted tumors were surgically removed and subsequently analyzed by immunohistochemistry and gene expression profiling, or used for the generation of PACO cultures. Animal care and all procedures followed the German legal regulations and were previously approved by the governmental review board of the state of Baden-Wuerttemberg, Regierungspraesidium Karlsruhe authorization numbers G64-10, G39-13, G105-14 and G80-15.

Cell culture. For the generation of PACO cultures, primary xenografts were resected after attaining a volume of approximately 1 cm^3. Tumor pieces were first minced using sterile scalpels and then dissociated into single cells by incubation with 1 µg/ml collagenase IV (Sigma) for 2 h at 37 °C. The resulting suspension was filtered through a 100 µM mesh, and cell debris and dead cells were removed by density centrifugation (FiColl Paque Plus, Amersham). The remaining erythrocytes were removed using ACK Buffer (Lonza). To establish PACO cultures, single cells (5×10^6) were seeded in T75 flasks (Primaria, BD) in serum-free medium (referred to as PACO medium) as described before[59]. PACO medium contains advanced Dulbecco's modified Eagle's medium–nutrient mixture F-12 (DMEM/F12; Life Technologies) with N2 supplement (Life Technologies), 50 ng/ml basic fibroblast growth factor (bFGF; Peprotech), 20 ng/ml epidermal growth factor (EGF; Peprotech), 10 ng/ml LONG R^3 insulin-like growth factor–I (IGF-I) (Sigma), 100 µM β-mercaptoethanol (Life Technologies), 2 µg/ml heparin (Sigma). Adherent monolayer cultures were maintained at 37 °C and 5% CO_2. After the outgrowth of tumor cells, contaminating fibroblasts were removed by trypsinization. We obtained SNU 5, SNU 16, KATO III, NCI N87, SK Hep1 and HepG2 cells from the American Type Culture Collection (ATCC).

Erlotinib-, dasatinib- and paclitaxel-resistant PACO cells were generated by continuously exposing cells to the individual compounds (10 nM or 20 nM) for 2 months. In brief, medium supplemented with the respective drugs was replaced every 4 d. At a confluency of 70%, cells were passaged and allowed to recover for 24 h until treatment was continued. Erlotinib, dasatinib or paclitaxel resistances were confirmed by dose-response studies as described below.

All cell lines used were authenticated monthly by single-nucleotide polymorphism profiling and tested for mycoplasma contamination (both by Multiplexion).

Sanger sequencing. Genomic DNA was prepared from PACO cells using DNAeasy Blood and Tissue Kit (Qiagen). Genomic DNA regions containing *KRAS* and *TP53* mutations were amplified by PCR using Q5 hot start high-fidelity master mix (New England Biolabs Inc.) according to the manufacturer's instructions. PCR primer pairs used are summarized in **Supplementary Table 10**. PCR products were purified using the High Pure PCR Product Purification Kit (Roche). Sanger sequencing was subsequently performed (GATC Biotech) and analyzed using ApE software, Version 2.0.49 (M. Wayne Davis; available for free at http://biologylabs.utah.edu/jorgensen/wayned/ape/). Variant positions are relative to the reference sequences NM_004985 (*KRAS*) and NM_000546 (*TP53*).

Gene expression analysis. Total RNA was isolated from different PACO lines at early and late passages at 80% confluency, or from 50 mg of tumor tissue using the miRNeasy kit (Qiagen) according to the manufacturer's instructions. Gene expression analysis was performed using Illumina HumanHT12v4 BeadChips at the Genomics and Proteomics Core Facility of the German Cancer Research Center (GPCF DKFZ, Heidelberg). Correlation plots, Spearman's rank correlation coefficients and significance (two-tailed) of $\log_2$ gene expression from the PACO data sets (PACO lines, primary (PT) and secondary (DT) xenografts) were generated using GraphPad Prism 6.0b software.

Gene set enrichment analysis (GSEA) was conducted on quantile-normalized data from the PACO and validation cohort data sets. In order to assign the corresponding PDAC subtype to the individual PACO samples, the previously described PDAssigner signature was used to derive gene sets for each individual subtype[11]. We computed *P* values using 1,000 or 10,000 permutations for each gene set and corrected them with the false-discovery rate (FDR) method[60]. We performed subtype assignment for the initial eight samples by comparing each individual sample against the remaining seven samples (designated REST) for each gene set. Samples were assigned to the signature and the respective subtype with the lowest FDR value (QM-PDA: PACO7, PACO9, PACO19; exocrine-like: PACO10, PACO14, PACO18; classical: PACO2, PACO17). GSEA was then repeated using the stratified groups for comparison. This initial cohort was used to identify surrogate protein markers for each subtype, and subsequent PDAC subtype classifications were marker based using immunohistochemistry.

RNA-seq by expectation maximization (RSEM[61])-normalized RNA-sequencing expression data of 183 primary PDAC tumors were obtained from The Cancer Genome Atlas (TCGA) PAAD data sets available online (Broad Institute). Spearman's rank correlation coefficients and significance (two-tailed) were calculated using GraphPad Prism 6.0b software for each pair of genes.

Gene expression data of the HIPO-015 xenograft validation cohort were quantile-normalized and corrected for unwanted variation using the 'fsva' function of the surrogate variable analysis (SVA) package[62,63]. Specifically, first, the number of latent factors ('surrogate variables') was determined by the function n.sv(). Then, the surrogate variables were estimated using the function sva() (with the subtypes as known covariates), and finally the function fsva() was used to regress out the surrogate variables and to obtain the corrected gene expression data. Probes mapping to multiple genes were excluded, and the first probe per gene was retained from the remaining set. Unsupervised principal component analysis (PCA) was then computed from the $\log_2$-transformed data using the 500 genes with highest variability across samples[64]. Calculations were performed by R Version 3.2.2.

The significance analysis of microarray (SAM)[65] was used to identify differentially regulated genes at an FDR < 0.05 with a fold change of >2. Additionally, differential expression of *CYP3A5* was validated based on $\log_2$-transformed mRNA expression data of the annotated xenograft samples from the validation cohort. Intensities of the probe with the highest average intensity per gene were retrieved from quantile-normalized microarray data. Unpaired *t*-test (two-tailed) was used to compute statistical significance ($P < 0.05$). Calculations were performed by R Version 3.2.2.

Hierarchical clustering analysis was performed on quantile-normalized, SVA-corrected, $\log_2$-transformed gene expression data of the validation cohort using R Version 3.2.2. Probes mapping to multiple genes were excluded, and the first probe per gene was retained from the remaining set. The intersection between the set of gene expression symbols and the previously determined PDAssigner gene set contained the variables used for hierarchical clustering with Manhattan distances and single linkage.

Microarray data are available in the ArrayExpress database (http://www.ebi.ac.uk/arrayexpress) under accession number E-MTAB-4029. The results shown

doi:10.1038/nm.4038

in **Supplementary Figures 1c** and **2n** are, in part, based upon data generated by TCGA Research Network (http://cancergenome.nih.gov/).

LC-MS/MS analysis. (*S*)-(−)-propranolol hydrochloride (internal standard) was purchased from Sigma. Acetonitrile was from Bernd Kraft (Duisburg, Germany); ammonium acetate and formic acid from Merck; methanol from VWR International; and dimethylsulfoxide from Applichem. 500 µl of reaction medium was quenched with 1,000 µl of acetonitrile at each time point and mixed. After centrifugation, clear supernatants were prediluted with PACO medium and acetonitrile at a ratio of 1:25. 100 µl of the sample was transferred into a new vial, 10 µl (*S*)-(−)-propranolol hydrochloride solution (105 µg/liter) was added, and the solution was vigorously mixed. Calibration and quality control samples were prepared by spiking PACO medium with either dasatinib or erlotinib. 10 µl of the samples was injected onto a PerfectSil Target ODS-3 HPLC column (3 µm, 100 × 2.1 mm, MZ-Analysentechnik), using an Agilent 1100 (Agilent) binary pump and degasser, with a CTC PAL sampler (CTC Analytics). Chromatographic separation was performed by gradient elution at a constant flow rate of 250 µl/min for 15 min. The gradient consisted of 20 mM NH_4OAc plus 0.1% formic acid (mobile phase A) and 400 mM NH_4OAc/methanol/acetonitrile (5:5:90) plus 0.1% formic acid (mobile phase B). The gradient applied was 0.0 min, 70% A–30% B; 1.5 min, 70% A–30% B; 3.0 min, 5% A–95% B; 11.0 min, 5% A–95% B; 11.5 min, 70% A–30% B; and 15 min, 70% A–30% B. From 4- to 8-min run time, the eluate was directed to a QTrap 5500 mass spectrometer (SCIEX) equipped with an electrospray ion source. Mass transitions of 488.1 to 401.1 for dasatinib, 394.0 to 278.1 for erlotinib and 260.1 to 116.1 for (*S*)-(−)-propranolol were monitored. Ionization was achieved at 5.5 kV and a temperature of 400 °C. Nitrogen was applied as curtain, collision and drying gas. Declustering potentials, collision energy and collision exit potential was as follows: 26 V, 39 V and 12 V for dasatinib; 16 V, 43 V and 26 V for erlotinib; and 61 V, 23 V and 14 V for (*S*)-(−)-propranolol.

Tissue microarray. The tissue microarray (TMA) was constructed from individuals that received partial pancreatoduodenectomy for PDAC between 1991 and 2006 at the Charité University Hospital Berlin. The use of this tumor cohort for biomarker analysis has been approved by the Charité University ethics committee (EA1/06/2004). Formalin-fixed and paraffin-embedded tissue samples were used to generate tissue microarrays as previously described[66]. Briefly, each PDAC sample included was represented by three different tissue cores, each measuring 1 mm in diameter and chosen by a board of certified pathologists as being representative for the respective tumor. From the defined regions, tissue cylinders of 1.5-mm diameter were punched from each donor sample and arrayed into a new 'recipient' paraffin block using a semiautomated tissue microarrayer (Beecher Instruments). The human various cancers high-density TMA, which is composed of VA2-SBC, VB2-SBC and VC2-SBC ($n = 438$), was purchased from Super Bio Chips (BioCat).

Immunohistochemistry and marker-based stratification. For a list of all marker candidates tested and a summary of the results obtained see **Supplementary Table 4**. Tumor specimens were fixed in 10% formalin overnight and embedded in paraffin. For immunohistochemistry, slides were deparaffinized and rehydrated. Antigen retrieval was enhanced by boiling in a steam pot at pH 6 in Dako target retrieval solution (Dako) for 15 min, followed by cooling for 30 min and washing in distilled water. Nonspecific binding was blocked by using the Linaris Avidin/Biotin blocking Kit (Vector Labs) according to the manufacturer's instructions. Slides were incubated with primary antibodies for 30 min, rinsed in PBS-T (PBS with 0.5% Tween-20), incubated for 20 min with the appropriate secondary antibody using the Dako REAL Detection System and rinsed in PBS-T. After blocking of endogenous peroxidase and incubation with streptavidin–horseradish peroxidase (HRP) (20 min at room temperature (RT)), slides were developed with AEC (Dako) and counterstained with hematoxylin. Primary antibodies and dilutions are described in **Supplementary Table 11**. All antibodies were diluted in Dako antibody diluent.

Three pathologists evaluated all of the sections independently; discordant cases were discussed using a multiheaded microscope until consensus was achieved. The study was carried out blinded as to the identity of the specimens. A case was considered positive for a given marker (CYP3A5, KRT81 and HNF1A) if the tumor cells in the respective tissue-microarray spots showed a detectable staining regardless of the strength of the signal or the number of positive cells. However, in those instances in which staining of tumor cells was detectable for any of the markers, the respective staining was usually strong. Hence, if any tumor cell was found positive for KRT81 or HNF1A expression in any of the cores, the tumor was defined as QM-PDA or exocrine-like, respectively. Stromal cells were negative in all instances; normal acinar pancreatic cells (when present) expressed HNF1A homogenously to a moderate degree but were consistently negative for the other two markers.

As whole-tissue slides were used in the validation cohort of xenografts, the scoring system was adapted to account for a higher level of heterogeneity, as observed in the samples stained for KRT81 and HNF1A. Specifically, a cutoff of at least 10% KRT81-positive tumor cells was introduced to consider a sample to be QM-PDA. Positive staining of a single tumor cell did not justify an allocation to a specific biological subtype. Additionally, the evaluation of HNF1A staining was adapted by only considering samples with moderate or strong nuclear staining reactions to be exocrine-like. A few cases with an extremely light nuclear staining reaction of HNF1A were observed, and these were not considered to represent biologically relevant HNF1A expression.

Immunofluorescence. PACO cells were seeded on T75 flasks (Primaria, BD) and grown to 60–70% confluency. Cells were fixed in 4% freshly depolymerized formaldehyde for 15 min, permeabilized with 0.25% (vol/vol) Triton X-100 (Sigma) in PBS for 45 min and blocked with 1% BSA in PBS for 1 h. Primary antibodies (**Supplementary Table 11**) were incubated overnight (O/N) at 4 °C, and detected by fluorescence using secondary antibodies coupled to fluorochromes (Life Technologies) that were diluted 1:1,000 and incubated for 1 h in the dark. Isotype-matched secondary antibodies conjugated with Alexa Fluor 488 or phycoerythrin (PE) were incubated for 1 h at room temperature (RT). Slides were mounted using ProLong Antifade GOLD with DAPI (Life Technologies), as described by the manufacturer.

Western blot analysis. Whole-cell lysates of PACO cells were prepared using RIPA buffer (Cell Signaling Technology), 1 mM PMSF (Sigma), 1 mM EDTA and Halt Protease-Phosphatase Inhibitor Cocktail (Pierce). Protein lysates were resolved on 4–12% Bis-Tris NuPage gels with MOPS running buffer (Life Technologies) and blotted on nitrocellulose membranes (Amersham International). Membranes were blocked for 1 h in TBS containing 0.1% (vol/vol) Tween-20 with 20% (wt/vol) nonfat dry milk powder (blocking solution). Primary antibodies (**Supplementary Table 11**) were incubated O/N at 4 °C in blocking solution. Secondary HRP-coupled antibodies (Southern Biotech) were diluted 1:10,000 in blocking solution and incubated for 1 h at RT. Membranes were washed in 0.1% TBS–Tween-20, and immunocomplexes were detected using the ECL kit (Amersham International). As positive controls, recombinant CYP3A5, CYP3A4, CYP3A7 (Abnova) and human liver lysates (Novus) were used.

Real-time quantitative PCR. Total RNA was extracted using the miRNeasy mini kit (Qiagen) and reverse-transcribed using the high capacity cDNA reverse-transcription kit (Applied Biosystems). cDNA corresponding to 10 ng of starting RNA was used for relative RNA quantification (qRT-PCR). TaqMan probes (Applied Biosystems) for *CYP3A5* (HS00241417_m1), *CYP3A4* (HS0060406_m1), *CYP3A7* (Hs00426361_m1), *HNF4A* (Hs00230853_m1), *NR1I2* (Hs01114267_m1), *PPIA* (HS04194521_s1) and *GAPDH* (HS9999905_m1) were used to acquire expression data with the Viia 7 Real-Time PCR System (Applied Biosystems). The ViiA 7 software 1.1 was used for data acquisition and analysis. As positive controls, RNA samples from total normal liver and pancreas were used (Novus).

siRNA transfection of PACO cells. PACO cells were grown to 80% confluency. The transfection reagent Dharmafect 4 (Thermo Scientific), non-targeting (siNT-control) and siRNAs targeting *CYP3A5*, *HNF4A* or *NR1I2* (On-Target plus SMARTpool Thermo Scientific; **Supplementary Table 12**) were pre-incubated at RT for 5 min at a ratio of 1:4 in IMDM culture medium (Gibco). For the *HNF4A* and *NR1I2* double-knockdown cells, the individual siRNAs were pre-incubated together at a ratio of 1:8 in IMDM culture medium (Gibco). Dharmafect 4

was then combined with the siRNAs and incubated for another 20 min at RT. The mixture was then added to the PACO culture medium. The culture medium was aspirated, and the transfection agent–RNA complex mixture was added to the monolayer. Flasks were incubated at 37 °C for 72 h until further analysis.

Generation of stable knockdown cells. Stable shRNA-mediated knockdown of *CYP3A5* was achieved by targeting the sequence 5′-TTGATTT CAACATCTTTCT-3′ in a pGIPZ vector (shCYP3A5) (GE Healthcare, Thermo Scientific; **Supplementary Table 12**). In addition the non-silencing control pGIPZ vector (shScr) was used as negative control (GE Healthcare, Thermo Scientific). Lentiviral particles were produced in HEK 293T cells (ATCC). Viral particles were concentrated and PACO cells were transduced at a multiplicity of infection of 1:5. Successfully transduced cells were selected by cell sorting for GFP. qRT-PCR and western blotting analyses confirmed knockdown efficiency.

Stable expression of *CYP3A5*. PACO cells were stably transduced with either the expression vector pLenti-GIII-CMV-RFP-2A-Puro (Applied Biological Materials Inc.) containing the full *CYP3A5* open reading frame ($CYP3A5^{OE}$) or an empty control vector (Ctrl). Lentiviral particles were produced in HEK 293T cells. Viral particles were concentrated, and PACO cells were transduced at a multiplicity of infection of 1:5. Successfully transduced cells were selected by cell sorting for RFP. qRT-PCR and western blotting confirmed *CYP3A5* expression.

Drug-treatment assays. Dasatinib, erlotinib and paclitaxel (LC Laboratories) were dissolved in water-free DMSO. For the determination of relative cell viability, 10 μM and 1 μM, or serial dilutions, of the three drugs were screened in quadruplicate. In brief, 8,000 cells/well were seeded in 96-well plates 24 h before the addition of the individual compounds. For the co-treatment experiments, either siRNA transfection was carried out as described or cells were pretreated with 100 nM ketoconazole for 2 h and then treated in the presence of ketoconazole. After incubation for 48 h or 7 d, cell viability was assessed using CellTiterBlue (Promega) following the manufacturer's instructions. Treatment with vehicle (DMSO) was used as a negative control. Treatment with 20 μM staurosporine (LC Laboratories) was used as a positive control. Responses were normalized to DMSO- and staurosporine-treated controls. Relative cell viability curves were plotted using GraphPad Prism 6.0b software.

***In vivo* drug treatment.** Tumors were established by subcutaneously injecting 5×10^5 shCYP3A5- or shScr-expressing exocrine-like (PACO10, PACO14) and classical (PACO17) cells into 8- to 12-week-old female NSG mice, using Matrigel (2 mg/ml) in a total injection volume of 100 μl. After the tumors reached a size of approximately 200 mm^3, mice were randomly assigned to the respective treatment groups ($n = 6$ per group) for drug administration. Erlotinib was prepared in 0.5% methylcellulose, 0.1% Tween 80 and 99.4% water for injection (WFI). Erlotinib (100 mg/kg) or vehicle was administrated by oral gavage for five consecutive days followed by 2 d of rest, for a duration of 14 d. Paclitaxel was prepared in 50% Cremophor EL (Sigma) and 50% absolute ethanol (Sigma) to a concentration of 6 mg/ml. Before administration, paclitaxel was further diluted in 0.9% NaCl (Braun) to a final concentration of 0.4 mg/ml. Paclitaxel (2 mg/kg) or vehicle was then administrated by intraperitoneal injection for two cycles of 5 d with paclitaxel and 2 d of recovery followed by 4 d with paclitaxel. Cells from one xenograft per treatment group were re-injected subcutaneously, and the mice were treated for two cycles of 5 d with paclitaxel and 2 d of recovery. Tumor volumes were determined (blinded; twice weekly by caliper measurements) and calculated according to the formula (length × height × width) × (π/6) at the end of the experiments. Tumor growth was calculated for each individual tumor by normalizing to the tumor volume at day 0. After 14 d or 18 d of treatment, mice were sacrificed and tumors were resected for further analyses. Mice were excluded if they had to be sacrificed before the treatment started or if tumor size exceeded the maximum allowable volume during the treatment experiment.

Statistical analysis. For all *in vitro* experiments, at least three biological replicates were used or grouped analyses were carried out. For all *in vivo* experiments, at least six mice per treatment group were used. Hence, for the reported differences, the sample size used gave sufficient power to call them reliable. Quantitative results were analyzed by one-way analysis of variance (one-way ANOVA), one-sided Mann-Whitney *U* test and Student's *t*-test using GraphPad Prism 6.0b software. Survival analysis was performed by using the Mantel-Cox log-rank test as well as the Cox proportional-hazards multivariate regression analysis using the Statistical Package for the Social Sciences (IBM SPSS software). Additionally, the Pearson chi-squared test was used for comparative data analysis, using SPSS. We considered $P < 0.05$ (two-sided) as statistically significant. For GSEA, a false discovery rate (FDR) of <0.2 was considered statistically significant. *In vitro* treatment data were evaluated by determining the activity area[29] from each dose-response curve by adding 'max' (100 − mean response, 0) for every concentration. Activity areas were compared by paired *t*-test. Calculations were performed in R Version 3.1.0 (ref. 67). Estimation of variation within each group was determined by s.e.m. or s.d.

59. Vermeulen, L. *et al.* Single-cell cloning of colon cancer stem cells reveals a multilineage differentiation capacity. *Proc. Natl. Acad. Sci. USA* **105**, 13427–13432 (2008).
60. Subramanian, A. *et al.* Gene set enrichment analysis: a knowledge-based approach for interpreting genome-wide expression profiles. *Proc. Natl. Acad. Sci. USA* **102**, 15545–15550 (2005).
61. Li, B. & Dewey, C.N. RSEM: accurate transcript quantification from RNA-seq data with or without a reference genome. *BMC Bioinformatics* **12**, 323 (2011).
62. Leek, J.T., Johnson, W.E., Parker, H.S., Jaffe, A.E. & Storey, J.D. The sva package for removing batch effects and other unwanted variation in high-throughput experiments. *Bioinformatics* **28**, 882–883 (2012).
63. Parker, H.S., Corrada Bravo, H. & Leek, J.T. Removing batch effects for prediction problems with frozen surrogate variable analysis. *PeerJ* **2**, e561 (2014).
64. Huber, W., von Heydebreck, A., Sültmann, H., Poustka, A. & Vingron, M. Variance stabilization applied to microarray data calibration and to the quantification of differential expression. *Bioinformatics* **18** (suppl. 1), S96–S104 (2002).
65. Tusher, V.G., Tibshirani, R. & Chu, G. Significance analysis of microarrays applied to the ionizing radiation response. *Proc. Natl. Acad. Sci. USA* **98**, 5116–5121 (2001).
66. Stenzinger, A. *et al.* High SIRT1 expression is a negative prognosticator in pancreatic ductal adenocarcinoma. *BMC Cancer* **13**, 450 (2013).
67. R Development Core Team. *R: A Language and Environment for Statistical Computing* (R Foundation for Statistical Computing, 2008).

doi:10.1038/nm.4038